Recycled hybrid fiber-reinforced & cement-stabilized pavement mixtures: Tensile properties and cracking characterization

Ahmed Hilal Farhan[1,]*, Andrew Robert Dawson [2], Nicholas Howard Thom [2]

[1] Department of Civil Engineering, College of Engineering, University of Anbar, Anbar, Iraq

Tel: +964 (0) 7700526388, E-mail: ahmed.farhan_ce@uoanbar.edu.iq,

ahmed.farhan2010@yahoo.com

[2] School of Civil Engineering, Faculty of Engineering, University of Nottingham, University Park, Nottingham, NG7 2RD, UK,

*Corresponding author.

Abstract

Cement-stabilized aggregate mixtures (CSAMs) have been used effectively within semi-rigid pavement structures. However, the sensitivity to cracking under tensile loading is the main problem that may cause a deterioration due to reflection to the overlaying layers. The primary objective of this research is to show the extent to which the steel fibers extracted from old tires might enhance the pre and post-cracking behavior of CSAMs and to understand how they affect the cracking characteristics. Mechanical performance was evaluated in terms of indirect tensile strength, modulus of elasticity, and post-peak load carrying capacity. Cracking properties were studied quantitatively, at the mesoscale level, using a combination of x-raying of the internal structure and fractal analysis through image processing technique. A new methodology was suggested and implemented for this evaluation. Despite the low cement content, results indicated a decrease in the material stiffness with fiber addition and an improvement in both pre- and post-cracking behavior. There is a clear enhancement in the toughness and deformability of the mixtures indicating a ductile material. Better cracking behavior was observed after fiber incorporation. Finer cracks and more dispersion of these cracks suggest a

reduced potential for reflection cracking. A fracture mechanism was proposed and confirmed by examining various cracking patterns.

Keywords: Cement-bound pavement mixtures; tensile testing; fiber-reinforced cement-stabilized mixture; fractal dimension; cracking characterization

1. Introduction

A cement-stabilized aggregate mixture (CSAM) is a cementitious material that consists of a mix of aggregate, cement and a small quantity of water for hydrating the cement and helping the compaction process (Lim and Zollinger 2003). It is normally used within semi-rigid pavements as a base and/or subbase layers to increase their structural capacity. Due to its low sensitivity to water and its high strength and uniformity, stabilized layers made of such material provide an excellent foundation to overlying layers. At the same time, stabilized layers protect the underlying layers by distributing the load over a wide area owing to their high rigidity.

Inherent features of CSAMs, however, are shrinkage and tensile cracking, low tensile strength and high rigidity which make them sensitive to overloading and fatigue. These cracks, unfortunately, cause a decrease in load-carrying capacity and transfer efficiency as well as problems for both overlying and underlying pavement courses. In addition to the additional stresses being applied on subgrades and wearing courses, reflection cracking represents a significant further challenge to the use of cement-stabilized layers (Adaska et al. 2004)

The use of fibers may provide a good solution to control the above-mentioned problems, especially in the light of findings of previous studies conducted on concrete mixtures. Furthermore, and more importantly, using these fibers might control crack initiation, propagation rate, and width. Apart from the idea that the cracks developed in a cement stabilized aggregate layer reduce its load carrying capacity, these cracks also cause problems, especially in the case of wide cracks, to other layers.

The use of fibers to reinforce CSAMs of low cement content is a relatively new technique as compared with normal concretes and few investigations have been performed to study the effect of fibers on the performance of cemented mixtures. Shahid (1997), Thompson (2001), Sobhan and Krizek (1999) and Coni and Pani (2007) all conducted studies to reveal how industrial steel fiber reinforcement affects the mechanical performance of cement-stabilized materials. Others (Khattak and Alrashidi 2006, Zhang and Li 2009, Zhang et al. 2010, Grilli et al. 2013) have used industrial polypropylene fibers. In all these studies, the host materials were either natural or secondary aggregates. Overall, their findings showed an improvement in the performance of cement-stabilized mixtures from the mechanical properties point of view.

Despite several advantages gained from fibers in cemented mixtures, their high initial cost represents a challenge that limits their use (Coni and Pani 2007). This was probably the main motivation for some researchers to attempt using waste fibers in cement-stabilized mixtures. For instance, Sobhan and Mashnad (2002) and Sobhan and Mashnad (2003) used a waste plastic strip as reinforcement in a cemented aggregate. Such usage helps to reduce the cost of construction and might also enhance the performance in addition to increasing sustainability in highway construction. Even in the case of concrete mixtures, only a few researchers (Aiello and Leuzzi 2010, Centonze et al. 2012, Sengul 2016, Leone et al. 2018) have tried to utilize steel fibers extracted from post-consumer tires as reinforcement.

No study has been reported in the literature investigating the effect of waste steel fibers sourced from old tires on the performance of cement-stabilized aggregate. Even though Angelakopoulos et al. (2015) and Neocleous et al. (2011) used these waste fibers in roller-compacted concrete, their mixtures had quite different aggregate gradation and much higher cement content as prescribed by the Portland Concrete Association (PCA 2005). Furthermore, none of the previous studies have examined the internal structure and cracking properties of such composites. Therefore, a study was undertaken, and is here reported, to investigate how the inclusion of waste steel fibers in cement-stabilized aggregate of low cement content (as compared with other cementitious materials) may affect its behavior.

Cement-stabilized aggregate layers (either base or subbase or both) within the pavement structure are subjected to tensile stresses at the bottom of the layer. This, in turn, suggests that a tensile test will best simulate actual, in-situ, distress. It would also be instructive to investigate the cracking properties and the internal structure at a mesoscale level so as to better understand the fracturing mechanism and to identify the relationship with macroscale properties. Therefore, the aim of the study is to quantify and understand the behavior of these composites in order to optimize them with the eventual goal of overcoming the disadvantages of cement-stabilized base pavements in a cost-effective manner.

2. Experimental Program

2.1 Constitutes materials

2.1.1 Aggregate

A crushed limestone aggregate was used during this investigation. This aggregate was sourced from Tunstead Quarry in Nottingham, UK at different fraction sizes which are 20 mm, 14 mm, 10 mm, 6 mm and dust. Grain size distributions for various stated fraction sizes was determined in accordance with BS EN 933-1:2012. Figure 1 illustrates the gradation of different aggregates.

2.1.2 Recycled fibers

Recycled steel fibers, extracted from post-consumer tires, were utilized as reinforcement in cement-stabilized aggregate mixtures. Due to the nature of the fibers used in the tire manufacturing and recycling process, the fibers produced after the tire shredding process have different diameters and lengths. To evaluate the behavior of fiber reinforced cement-stabilized aggregate mixtures (FRCSAMs), it is necessary to quantify the fibers' geometrical properties. This is because the interlocking of the fibers with the aggregate and the bond strength of the fibers with the matrix is expected to be highly related to the fiber length in addition to the cement content. Therefore, both fiber diameter and length were characterized to help understand the effect of different geometrical properties of the fibers on the performance of modified mixtures, as different fiber properties may result in different performance.

To achieve this fiber quantification, a random fiber sample was taken from different locations of the fiber container. To measure the fiber diameters, a digital micrometer with a total range between 0 and 2.5 mm and a precision of 0.001 mm was used (Figure 2). Regarding fiber lengths characterization, an image processing technique was adopted through the following procedure: firstly, the fibers were distributed on a white board as batches in such a way as to ensure the fibers were isolated from each other. Then, pictures were captured for each batch utilizing a high-resolution camera. After that, these images were inserted into a CAD environment and scaled up to reflect the actual dimensions in millimeters. From CAD software tools, fiber lengths were measured.

Results showed a bimodal distribution of the fibers' diameters as illustrated in Figure 3. Around 20.53%, 12.15%, 29.89%, and 15.27% of the fibers have a diameter about 0.2-0.25 mm, 0.15-0.20 mm, 0.35-0.40 mm and 0.40-0.45 mm, respectively. With regards to fibers' lengths, on the contrary, there is a unimodal distribution of this parameter where the majority of the fibers (around 63.15%) have a length range between 35 and 40 mm. This majority is distributed as follows: 24.01%, 21.71%, and 17.43% have a length range of 35-40 mm, 30-35 mm and 40-45 mm, respectively.

Comparing and contrasting this geometrical characterization of fibers with those attempted in the previous studies, Caggiano et al. (2015) and Caggiano et al. (2017) indicated similar distributions where either bimodal or multimodal distributions and a unimodal distribution were obtained for the fibers' diameters and lengths, respectively. Martinelli et al. (2015) and Caggiano et al. (2017) attributed the unimodal distribution of the fiber length to the uniform process by which the shredding machines cut the fibers whereas the multimodal/bimodal distribution of the fiber diameters results from the mixed types of tires i.e., passenger car, buses and truck tires.

2.1.3 Other constituents

Portland cement (CEM I 52.5 N) was used to bind the aggregates at a cement content of 7% by weight of aggregate and fibers. This was selected based on the highest cement content used in previous studies (Farhan et al. 2016) to stabilized the aggregate mixtures. The highest level was chosen to provide enough bond strength between fibers and the surrounding materials. The aggregate-cement mixture was moisturized utilizing tap water.

2.2 Mix design

As is well known, the performance of cement-stabilized aggregate is largely governed by its density which, in turn, partly depends on aggregate gradation. Consequently, the aggregate mixture was batched individually for each sample to ensure comparable specimens i.e., to eliminate any variability resulting from aggregate gradation change. Aggregate fraction sizes were blended in different proportions (13% of 20 mm, 18% of 14 mm, 16% of 10 mm, 13% of 6 mm and 40% of dust) in such a way as to ensure production of Cement Bound Granular Mixture 2-0 described in BS EN 14227-1:2013. The fabricated gradation is shown in Figure 1.

In their investigations, Shahid (1997) and later on Thompson (2001) used industrial steel fibers at a maximum volumetric content of 1%. Therefore, the same maximum fiber level was used in this study. However, initial trials attempted during the course of this investigation showed a difficulty in homogeneous dispersion of the fibers at this maximum level due to the occurrence of balling and agglomeration. Consequently, the fiber content was limited to 0.75% by volume of aggregate. In addition to the reference mix, fiber-reinforced mixtures containing 0.25%, 0.50% and 0.75% by volume of aggregate were studied. Similar fiber reinforcement levels have been investigated in concrete mixtures as reported in Aghaee et al. (2015).

Since the aggregate was identical, in terms of type and gradation, with that used by Farhan et al. (2016), the same cement and water contents were adopted, namely 7% (by dry weight of aggregate) and 4.7% (by dry weight of aggregate and cement), respectively, for the reference mix containing no fibers. Concerning fiber-reinforced mixtures, cement and water contents were proportioned on the basis of the dry weight of aggregate and fibers and the dry weight of aggregate, cement, and fibers, respectively. Although volumetric proportioning of cement and water should in theory be adopted, especially in the light of the large differences between the specific gravities of fibers and aggregates, using a weight basis to determine these amounts is suitable for such low percentages of fibers, cement, and water. The differences are negligible and within the accuracy of the batch process taking into account that each sample was batched, mixed and compacted separately. A vibrating hammer was used for compaction of specimens as described in BS EN 13286-4:2003.

To designate the different mixtures, two letters (C and F to indicate cement and fibers, respectively) are each followed by a number to indicate the component (either fibers or cement) content used. For instance, the mixture stabilized with 7% cement and reinforced with 0.5% fibers, will be described as C7F0.5.

2.3 Specimen fabrication and curing

Mixing of various components was carried out manually. Dry aggregates of different fractional sizes were mixed with cement for one minute. After that, the designed water content was added and the wet aggregate-cement mixture was further mixed for two minutes. Finally, a further one-minute mixing was performed after fiber addition.

The final mix was compacted in two layers using a vibrating hammer (Kango 638) in oiled steel molds to manufacture 100 mm x 100 mm cylindrical specimens. The compacted specimens were left in their molds overnight and then demolded, wrapped with cling film and placed in wet plastic bags. After a 28-day curing period, samples were unwrapped and trimmed with a diamond saw to obtain a height of exactly 100 mm ready for testing (Figure 4). It can be seen from this figure that no pulling-out of the fibers occurred during the sawing process which might suggest a good bond and/or interlocking between the fibers and adjacent aggregate.

2.4 Testing methodologies

2.4.1 Tensile strength and density

Cement-stabilized base courses within a pavement structure are always designed based on tensile stress at the bottom of the layer. Therefore, the effect of fiber reinforcement was evaluated in terms of tensile properties. Also, the classification of cement stabilized aggregate mixtures is conducted based on the tensile strength of the mixture as described by BS EN 14227-1:2013. In this study, the indirect tensile test was performed at 28-days on an Instron testing machine with a capacity of 200 kN based on BS EN 13286-42:2003. Three of the 100 mm dia. x 100 mm height specimens were manufactured and tested. Indirect tensile strength (ITS) was computed as

$$\mathrm{ITS} = \frac{2P}{\pi h d} \qquad (1)$$

In the above equation, ultimate load in Newtons and specimen thickness and diameter in millimeter are denoted by P, h and D, respectively. Density was measured using the water-displacement method.

2.4.2 Load-diametrical deformation curves and static elasticity modulus

Simultaneously with ITS measurement, lateral deformations were captured using a linear variable differential transformer (LVDT) to construct the load-deformation relationships necessary to estimate modulus of elasticity and toughness. Figure 5 shows the instrumented ITS test setup used in this paper. Deformation was controlled at a rate of 0.5 mm/min. Based on BS EN 13286-43:2003 recommendations, 30% of the ultimate load and its corresponding deformation were used to estimate static modulus of elasticity. However, due to the differences in gauge distance resulting from the different LVDT arrangements between the above-mentioned specification and that employed in this paper, Solanki and Zaman (2013)'s equation was adopted in moduli calculations instead of the one stated in BS EN 13286-43:2003, as follows:

$$E_t = \frac{2P}{\pi.D.h.\Delta H(D^2+D_G^2)}\left\{(3+\upsilon)D^2.D_G + (1-\upsilon)\left[D_G^3 - 2D(D^2+D_G^2)\tan^{-1}\left(\frac{D_G}{D}\right)\right]\right\} \quad (2)$$

where E_t= static modulus of elasticity measured in indirect tensile mode, P= 30% of maximum sustained load; D=diameter of the specimen; h= thickness of specimen; ΔH=lateral deformation at 30% of ultimate load; D_G= gauge distance and υ = Poisson's ratio.

2.4.3 Absolute toughness and ductility

To assess the load-bearing capacity in the post-peak zone or toughness of the reinforced mixtures, the area under the load-deformation curve was estimated (Shahid 1997). As reported by Sobhan and Mashnad (2000), such estimation takes into consideration the enhancement of both strength and ductility due to fiber reinforcement.

Ductility, on the other hand, was quantified in terms of the deformability index (D_i) proposed by Park (2011) as

$$D_i = \Delta_{reinforced} / \Delta_{unreinforced} \tag{3}$$

where $\Delta_{reinforced}$ and $\Delta_{unreinforced}$ are the deformations at ultimate load of fiber-reinforced and unreinforced specimens, respectively.

3. Findings and discussion

3.1 Effect of fibers on indirect tensile strength and density

Figure 6 illustrates the effect of fiber reinforcement on the ITS value of cement-stabilized aggregate mixtures. Ultimate tensile strength improved by 22%, 40%, 50% due to fiber inclusion at volumetric contents of 0.25%, 0.5% and 0.75%, respectively. Despite the low cement content used in CSAMs compared with that of normal concrete, it seems that the interlocking with the aggregate particles represents another mechanism for activating the fiber reinforcement. In his study, Thompson (2001) used industrial steel fibers in cemented aggregate and reported a lower degree of improvement, with about 30% and 40% improvement due to 0.5% and 1% volumetric fiber contents, respectively. The greater enhancement reported in this paper can be attributed to the hybrid fiber reinforcement of different fiber lengths and diameters. This explanation was inspired from Betterman et al. (1995) who reported that the presence of hybrid fiber reinforcement ensures better performance. They considered that the improvement of tensile strength is governed by the presence of microfibers whereas the larger fibers are responsible for the enhancement in the post-peak zone. Another contributory factor in this greater enhancement is the degree of fiber dispersion inside specimen where, for the same fiber content, the number of fibers used by Thompson (2001) is much less than that used in this study. This is because the length and diameter of the industrial fiber used by the latter author is 60 mm and 0.9 mm, respectively, which are greater than these of fiber used here (Section 2.1).

Therefore, this led to better dispersion of the fiber in current study which means better internal stress resistance at both micro- and macro scale levels.

These findings confirm that the use of cheap waste steel fibers can improve the tensile strength of cemented mixtures to a similar level or better than that achieved by relatively expensive industrial steel fibers. This leads to more economical reinforcement for this mixture type while still achieving improved mechanical performance.

Regarding the measured density, fiber addition caused an increase in this parameter as shown in Figure 7. This is logical since the density of steel fibers is more than that of the limestone aggregate. Therefore, the maximum increase of 0.8% in density that occurred at 0.75% fiber content does not necessarily mean an increase in compaction efficiency but this increase could be due to the differences in specific gravities of mixture components (i.e., fiber and aggregate). Most importantly, incorporating of these steel fibers at the mentioned contents seems have a negligible effect on compaction efficiency of the stabilized mixture. In fact, calculating material packing changes (based on the overall density and fiber percentage changes) indicates that there is a small decrease in aggregate packing density (around 0.76%) although this may be within the inherent variability that can be expected.

3.2 Effect of fibers on load-deformation curves and moduli of elasticity

Figure 8 demonstrates the load-deformation relationships for different investigated mixtures. Unlike the unreinforced cement-stabilized aggregate mixtures (CSAMs) where the deformation-softening occurs immediately after the first crack formation, in all FRCSAMs there is a deformation-hardening zone following the first crack point. The deformation-softening then occurred gradually. In addition, it can be seen that for the reinforced mixtures, the deformation at peak load is much higher than for unreinforced mixtures which indicates a more ductile behavior.

Reduced mixture stiffness were obtained with fibers incorporation; Figure 9 shows that the moduli of elasticity of the FRCSAMs are lower than that of the CSAM. Adding volumetric fiber content of 0.25%, 0.5%, and 0.75% reduced the modulus of elasticity to 57%, 75% and 54% that of the unreinforced mixture. The fluctuation in this stiffness reduce may possibly be attributed to differences in fiber distribution. Nevertheless, the fibrous mixtures are always less stiff than the unreinforced materials.

3.3 Effect of fibers on toughness and ductility

In general, it can be inferred, based on the findings illustrated in Figure 10, that the greater the fiber-content the greater the toughness of the fiber-modified mixture. The range of toughness improvement is between 174 and 359%. This indicates that FRCSAMs tend to absorb more energy before failure compared with non-reinforced mixtures.

Regarding ductility, Figure 11 shows that the deformation indices are always greater for reinforced mixtures as compared with those for mixtures containing no fibers. Compared with the unreinforced mixture, deformability increased 12, 10 and 7 times when fiber content of 0.25%, 0.5%, and 0.75%, respectively were incorporated. The largest ductility occurred at 0.25% fiber content, then a decrease was experienced at higher reinforcement levels. Kim et al. (2010) reported similar behavior when they studied different fiber levels in normal concrete mixtures. They concluded that the ductility was significantly improved after fiber inclusion and the best ductility occurred at the lowest investigated reinforcement level. The reason behind this behavior might be due to the relatively heavy reinforcement at 0.5% and 0.75% fiber content, which might restrain the specimen from showing more deformation at failure.

3.4 Suggested fracturing mechanism

A possible explanation for the observed behavior is that when the micro-cracks first develop, fibers tend to arrest their propagation and to reduce the stresses at cracks tips. This means that the fibers absorb the energy generated to propagate these cracks. At this stage, the specimen still carries additional tensile load due to the combined effect of binder (cement) and aggregate-fiber interlock, as clearly shown from load-deformation curves (Figure 8). At the same time, deformation occurs as a result of deterioration of the bond between fibers and adjacent materials and slippage of the fibers. With continuing load application, there is more energy dissipation to deteriorate the bond between fibers and their surrounding components or to fail those fibers in the path of a crack. Since fibers inhibit the propagation of cracks, other cracks tend to develop toward the weakest directions which, in turn, results in cracks branching and more dispersion of these cracks inside the fractured sample. After the ultimate load has been reached, the macro-cracking stage begins, but a bridging effect due to fibers still exists. This would explain the load carrying capacity in the post-peak zone. Hence, it can be said that the fracture of FRCSAMs might be largely governed by the fiber distribution inside these mixtures. This suggested fracturing mechanism will be examined later.

4 Damage assessment at mesoscale level

The sensitivity of cement-stabilized aggregate mixtures to shrinkage or load-induced cracking represents one of the most important (if not the only) issue. Therefore, evaluation of the cracking patterns and damage characteristics is necessary to best evaluate and understand the usefulness of fiber reinforcement and also to support the proposed fracturing mechanism. This has been conducted quantitatively, at a mesostructure level, in terms of fractal analysis. As the uniformity of fiber distribution is expected to control both crack initiation and propagation and might lead, as reported by Zhang and Li (2009), to an improvement in the strength of the composite, the distribution of the steel fibers within the CSAMs has also been evaluated.

To enable this analysis, the damaged samples were first x-rayed (Figure 12) using a mini focus system having an x-ray source of 300 kV and a linear detector. Five equally spaced CT scans were captured for each sample at a resolution of 0.065 mm/pixel. Samples of these scans are illustrated in Figure 13.

4.1 Fractal analysis, fracture energy, and their distributions

In previous studies, fractal analysis has been used to investigate damage of concrete mixtures (Issa and Hammad 1994, Carpinteri et al. 1999, Yan et al. 2002, Guo et al. 2007, Erdem and Blankson 2013, Yang et al. 2017), asphaltic mixtures (Hassan 2012) and cement-stabilized mixtures (Farhan et al. 2016). Authors of these studies adopted the surface macro-crack or the fractured surfaces to estimate either one-dimensional (1D) or, more precisely, three-dimensional (3D) fractal dimensions. Fractal dimension identifies, quantitatively, the irregularity of surface cracks which helps to identify the propagation patterns of these cracks. In the current study, due to the expected variations in fiber distribution, variation in the cracking patterns along the sample height is likely, which may necessitate, for better accuracy, the determination of the fractal dimension through the sample height rather than adopting the surface macro-crack used in past studies. Finding the 3D fractal dimension based on the fractured surface is impossible for the current study due to the local crushing and/or non-splitting of the specimen (due to the fiber bridging effect) as shown in Figure 14. Therefore, a new methodology for estimating the 2D fractal dimension based on the combination of in-depth macro-crack and x-ray computed tomography is suggested and implemented in this paper for the first time. In this methodology, fractal dimensions were estimated from individual images of each sample through an image processing technique utilizing ImageJ software. The box-counting method was employed for fractal dimension estimation. Then, the distribution of the fractal dimension along the sample height and the average value were calculated.

Guo et al. (2007) proposed and used the following formula for rough estimation of the fracture energy from the computed fractal dimension:

$$W_s/G_f = a * (\delta/a)^{1-D_{1-d}} \quad (4)$$

where the energy dissipated at the crack surface is denoted as W_s, At the observation scale (δ) the fracture energy is G_f, a is the euclidean length which is taken as the diameter of the specimen and D_{1-d} is the estimated fractal dimension. Therefore, the corresponding fracture energies were also calculated and the fracture energy profile along the sample and the average value were also estimated.

4.2 Fibers distribution and cracking density

An image processing technique in ImageJ software was utilized to estimate fiber distribution and cracking density along the specimen height. Firstly, the CT scan images for each sample were inserted into the ImageJ environment. Cropping, filtration and image enhancement were conducted using software tools. For a meaningful comparison, the inserted images were calibrated to convert dimensions from pixels to actual dimensions. Next, different thresholds were used to separate the fibers from the other components and then to separate the cracking area. In this process, since one of the components of the X-ray images is the air-voids, it was difficult to separate them from the cracked area where both have similar dark color (Figure 13). To overcome this problem, these air-voids were tracked and deleted before binarization of the CT scan images.

4.3 Effect of fibers on damage and mesostructural properties

Figure 13 and Figure 14 show the cracking patterns of different fiber contents. It can be seen that the cracking seems of less width as the fiber content increases. This may suggest that the load transfer efficiency is much better in the case of reinforced as compared to non-reinforced mixtures. This load carrying capacity, in fact, comes from two components. The first is the crack bridging effect of the fibers that ties the cracked blocks together. The second is the improved aggregate interlock across the cracks due to limited crack width. This component is highly influenced by crack width as reported by Shahid (1997). Another important conclusion that can be inferred from Figure 14 is the mode of failure for different mixtures. Failure is a combination of tensile failure (due to the maximum tensile stress occurring perpendicularly to the loading strip) and local crushing underneath the loading strip. This suggests that the indirect tensile test, in the case of fibre-reinforced mixtures, might underestimate the tensile strength of those mixtures and/or the tensile stress carrying capacity beyond the ultimate strength. The apparent reduced capacity (see Figure 8) after peak load might be due to wedge formation/local crushing at the loading point (Figure 14) rather than loss of tension-sustaining capacity. The behavior in the post-peak zone appears to be predominantly governed by this local crushing/wedge formation which makes it difficult to quantify the actual toughness as reported by Thompson (2001). Thus, the actual toughness might be underestimated.

Regarding fiber distribution along the specimen height, it can clearly be seen from Figure 15a that the more the fiber content, the more the fluctuation in the distribution of fibers. It seems that the presence of fibers caused a disorder in cracking regardless of fiber content, as shown in Figure 15b. Fractal dimension distributions through different samples are illustrated in Figure 15c. This figure reveals that the addition of fibers increases the fractal dimension which confirms an improvement in the dispersed nature of the cracks. Regarding the fractal dimension distributions, the reference stabilized mixture showed a lower degree of variability along the sample height as compared with fiber-reinforced mixtures. The distribution in the latter mixtures fluctuated, which in turn indicates variability in the damage patterns. These findings might suggest a change to the cracking patterns after fiber-reinforcement of stabilized mixtures and confirms an increase in crack tortuosity. Yan et al. (2003) attributed the higher fractal dimensions to the higher degree of crack disorder during load application. This supports the suggested fracturing mechanism (Section 3.4)

Fracture energy estimated on the basis of in-depth macro-cracks also increased as shown in Figure 15d. This seems consistent with the improvement that occurred in the toughness or absorbed energy computed on the basis of load-deformation relationships (Figure 10). Apart from the variability within fiber-reinforced mixtures, both approaches confirm higher fracture energy in FRCSAMs compared with non-reinforced CSAMs. Table 1 illustrates the average fractal dimensions, fracture energies and cracking densities for different mixtures. The general trend observed from this table is that the addition of fibers causes an increase in the above-mentioned parameters. Fractal dimension is well correlated with macro-structural properties (ITS and modulus of elasticity) as shown in Figure 16. In one study by Yan et al. (2002) on the flexural-induced cracking of fiber-reinforced concrete, fractal dimension estimated on the basis of surface-macro cracks was also well correlated with both compressive and flexural strengths.

Overall, the tortuous cracks combined with the fiber bridging effect results in an improvement in the load transfer capacity after crack initiation and formation. The distribution of cracks over a greater area rather than individual, concentrated cracks might help to reduce the reflectivity of the cracks which will lead to less need for maintenance and should improve the riding quality and ensure more durable pavements.

5 Practical implications

In terms of stress ratio (the applied stress at the bottom of a stabilized layer divided by its strength) as used in pavement design in accordance with the mechanistic-empirical philosophy, an increase in tensile strength due to steel fiber inclusion will cause a decrease in stress ratio and thus an increase in fatigue life or decrease in pavement thickness. Regarding load transfer capacity, the bridging effect of the fibers will provide an excellent load transfer mechanism between pavement blocks after crack formation. Furthermore, such a bridging effect will also keep cracks narrow which, in turn, leads to less reflection cracking potential; hence, a delay in the deterioration of the pavement structure and also less frequent maintenance. Considering the high cost of industrial fibers, incorporating waste fibers is an attractive option and can be justified from two points of view. Firstly, the cost of such waste fibers is much less than industrial fibers. Secondly, the use of fibers will ensure savings in layer thickness and at the same time reduce maintenance frequency.

6 Conclusions

The impact of sustainable reinforcement of cement-stabilized aggregate mixtures with recycled steel fibers was investigated. The performance was evaluated in terms of tensile properties. Cracking damage and internal structure were quantified at a mesoscale level to better understand the behavior and fracture mechanism in combination with the macro-scale properties. The main conclusions inferred from the study could be summarized as follows:

1. Indirect tensile strength improved noticeably due to recycled steel fiber inclusion. ITS increased linearly with the amount of fibers. From a mechanistic pavement design point of view, this will reduce the required pavement thickness or reduce the maintenance needs. Regarding the rigidity of the cemented layer, fiber addition produces less stiff materials such that the elastic modulus reduced after fiber reinforcement.

2. Toughness and deformability of the fiber-reinforced cemented composite improved significantly, which confirms that it is a more ductile material and suggests improved fatigue behavior. Post-failure decay of pavements constructed of such a material can be expected to be less rapid, which may be helpful in maintaining lifeline access when maintenance intervention is not forthcoming.

3. Fractal analysis revealed a greater fractal dimension when fiber-reinforced mixtures compared with mixtures without fibers. This conclusion is valid through the sample height, indicating more homogenous crack dispersion.

4. Despite the lower cement content (as compared with normal concrete), the fibers still improve mechanical properties and cracking behavior. This might suggest that the bond between fibers and surrounding materials is not the only mechanism of improvement, but that the interaction and interlocking with the aggregate is another mechanism enhancing behavior. Therefore, it is recommended to quantify the extent to which these two mechanisms and their interaction might affect the final performance of the reinforced and compacted cement-stabilized mixtures.

5. No direct relation was observed between fiber distribution and damage properties. Nevertheless, the presence of fibers along the sample height caused disordered cracking and more dispersion of these cracks which may reduce reflection cracking in the pavement structure. This was supported by quantitative characterization of the internal structure.

6. The suggested methodology for calculating the fractal dimensions along the specimen on the basis of CT scans seems effective and more representative for quantitative identification of the cracking patterns and propagation and also for accurate estimation of fractal dimension and fracture energy distribution along the specimen.

Acknowledgements

The authors would like to acknowledge the support from the University of Nottingham. Thanks are also extended to Mr. Nigel Rook, Mr. Richard Blackmore, the Senior Technicians of the Civil Engineering Department and Mr. Chris Fox, the Senior Experimental Officer at the same university for helping in the experimental program.

Figure Captions

Figure 1: Gradation of individual aggregate fraction sizes, aggregate mix and specification.

Figure 2: Recycled steel fiber appearance and diameter measurement process

Figure 3: Fibre geometrical properties: a. fiber lengths; b. fiber diameters

Figure 4: Specimens after demoulding and trimming.

Figure 5: Close-up view of indirect tensile testing setup.

Figure 6: Effect of fiber content on indirect tensile strength.

Figure 7: Measured densities for fiberized mixtures.

Figure 8: Load-diametrical deformation curves for different fiber levels: a. C7F0; b.C7F0.25; c. C7R0.5; d.C7R0.75 (three specimens for each mix).

Figure 9: Elastic modulus for different fiber contents.

Figure 10: Absolute toughness for investigated mixtures.

Figure 11: Deformability indices for various investigated mixtures.

Figure 12: X-raying tensile-induced failed samples.

Figure 13: X-ray sample images of failed specimens: a. C7F0; b. C7F0.25; c. C7F0.5 and d. C7F0.75

Figure 14: Failure modes for various investigated mixtures: a. C7F0.25; b.C7F0.5; c. C7R0.75

Figure 15: Damage and mesostructure properties: a. Fiber distributions, b. cracking density distributions, c. fractal dimension distributions and d. Fracture energy distributions

Figure 16: Correlation of fractal dimension with ITS and elastic modulus.

Figure 1: Gradation of individual aggregate fraction sizes, aggregate mix and specification.

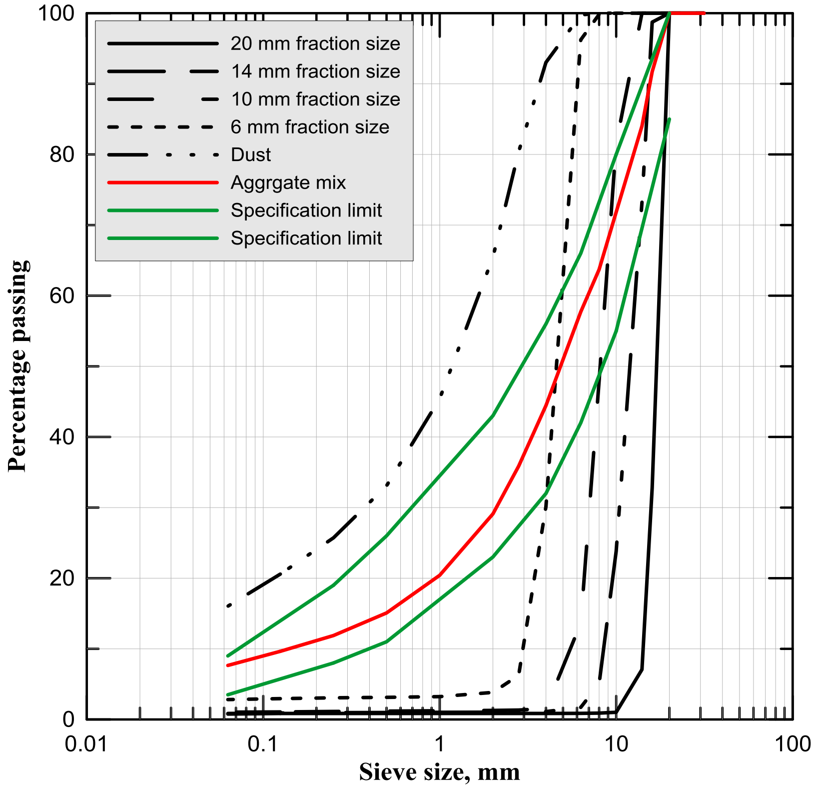

Figure 2: Recycled steel fiber appearance and diameter measurement process.

Figure 3: Fibre geometrical properties: a. fiber lengths; b. fiber diameters.

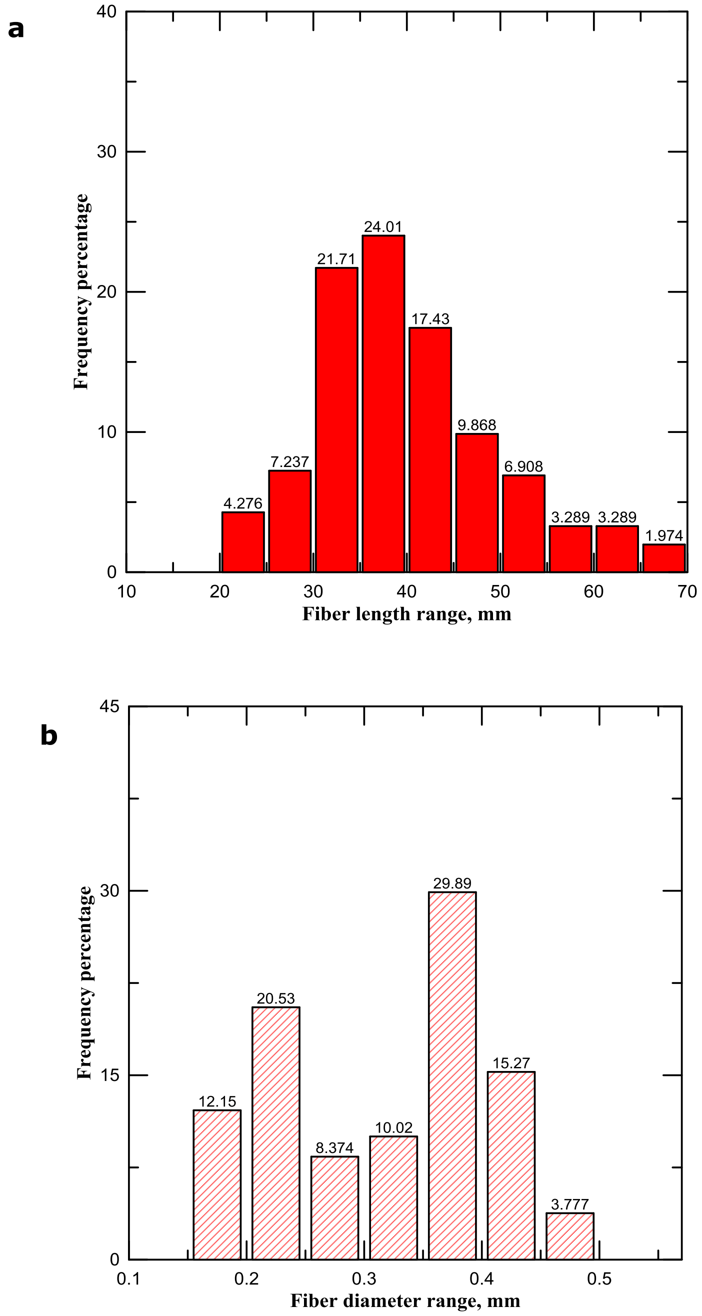

Figure 4: Specimens after demoulding and trimming.

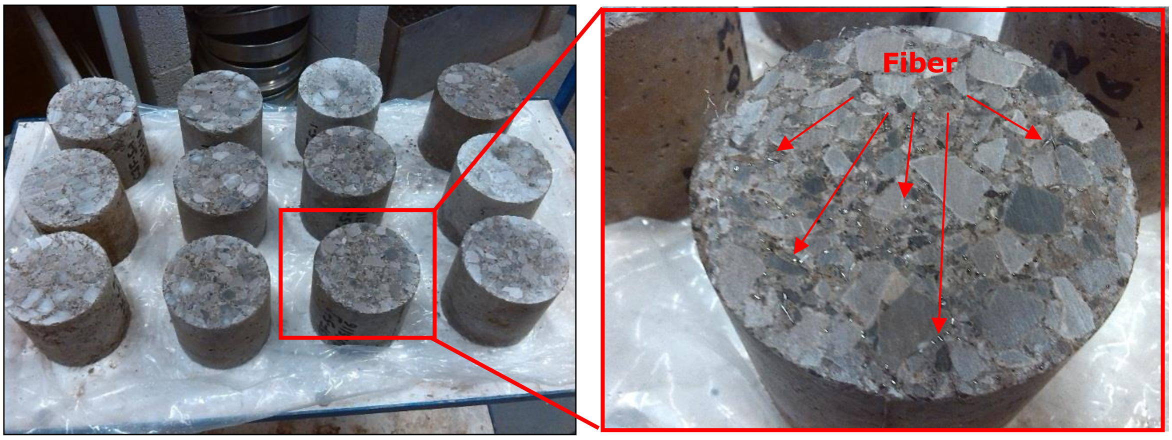

Figure 5: Close-up view of indirect tensile testing setup.

Figure 6: Effect of fiber content on indirect tensile strength.

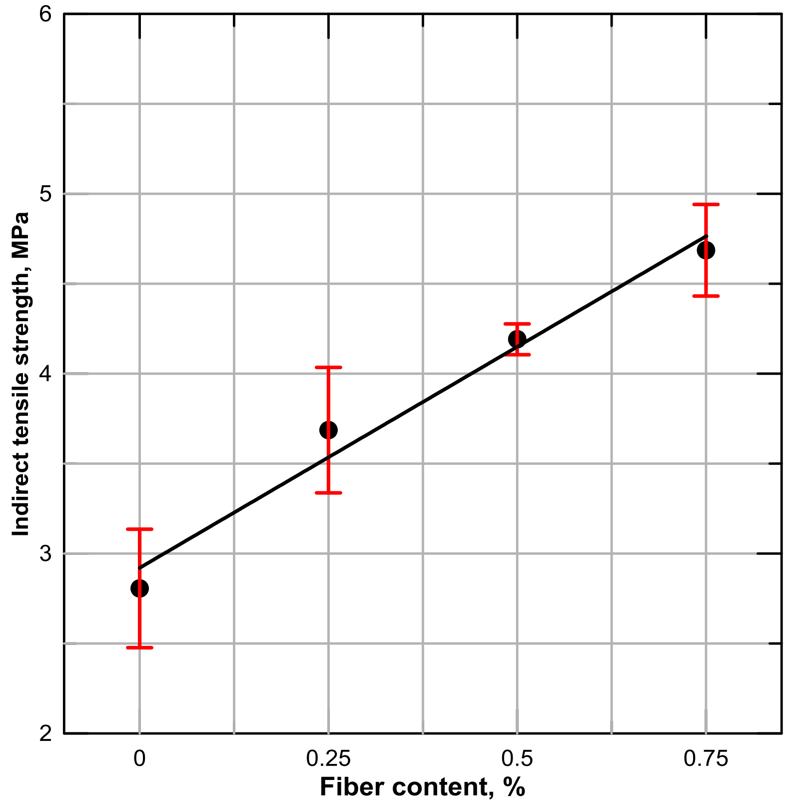

Figure 7: Measured densities for fiberized mixtures.

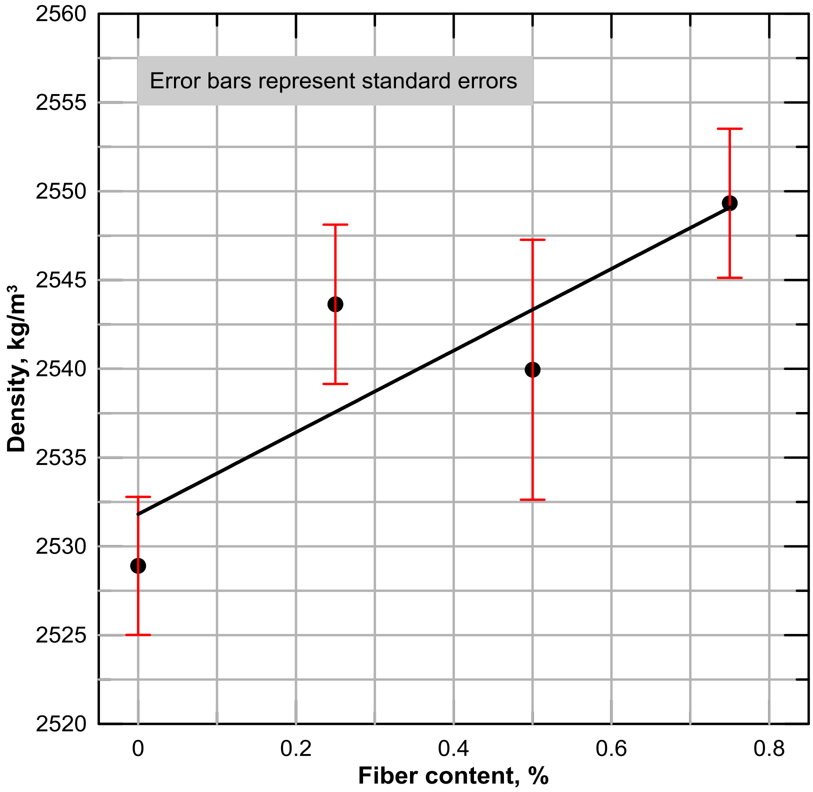

Figure 8: Load-diametrical deformation curves for different fiber levels: a. C7F0; b.C7F0.25; c. C7R0.5; d.C7R0.75 (three specimens for each mix).

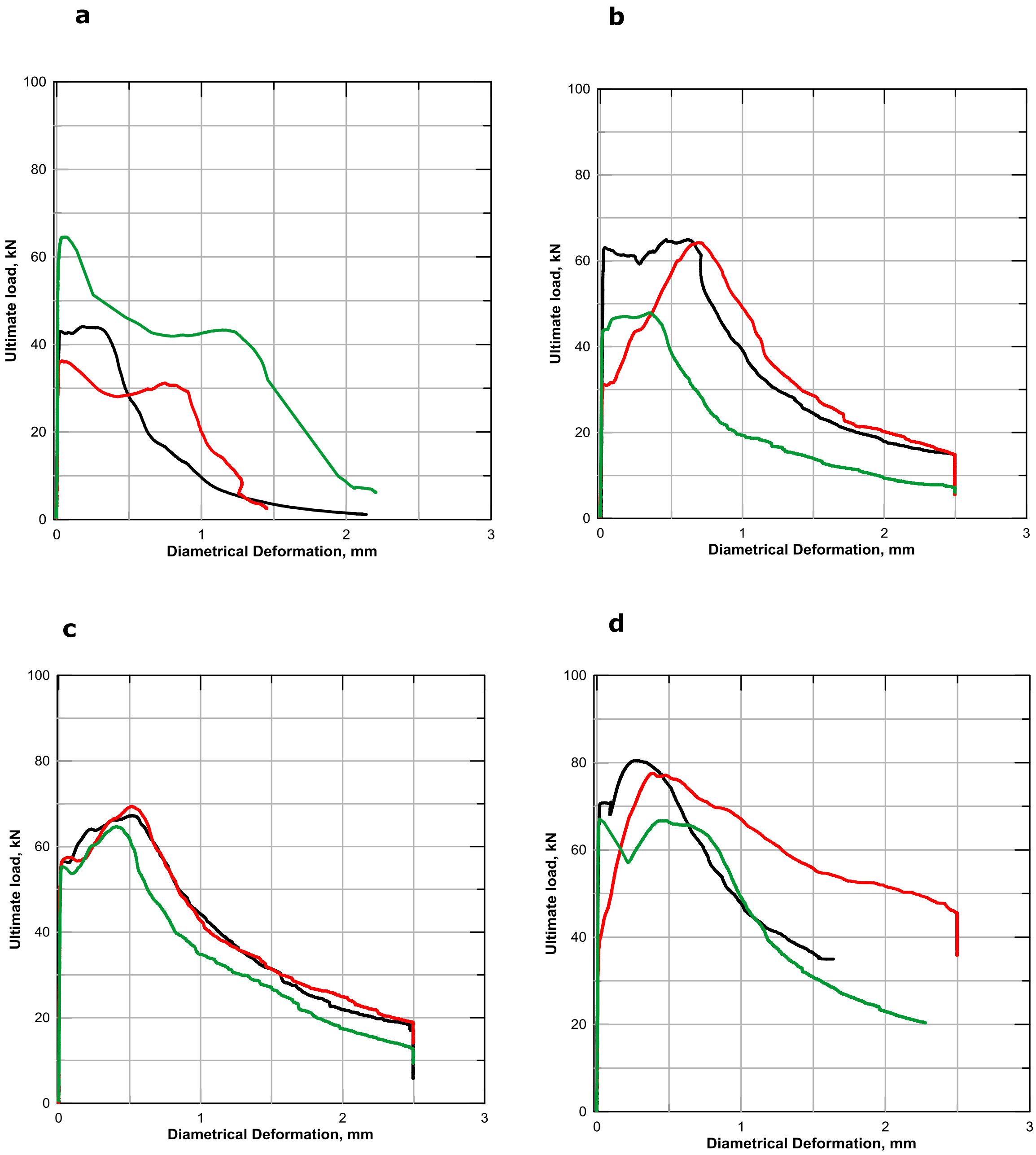

Figure 9: Elastic modulus for different fiber contents.

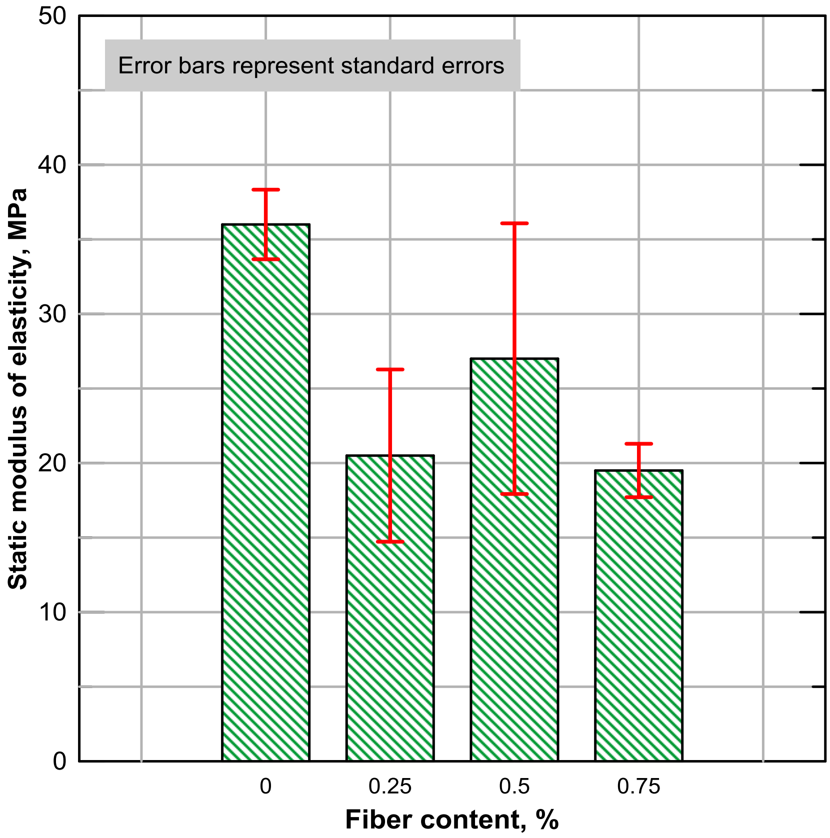

Figure 10: Absolute toughness for investigated mixtures.

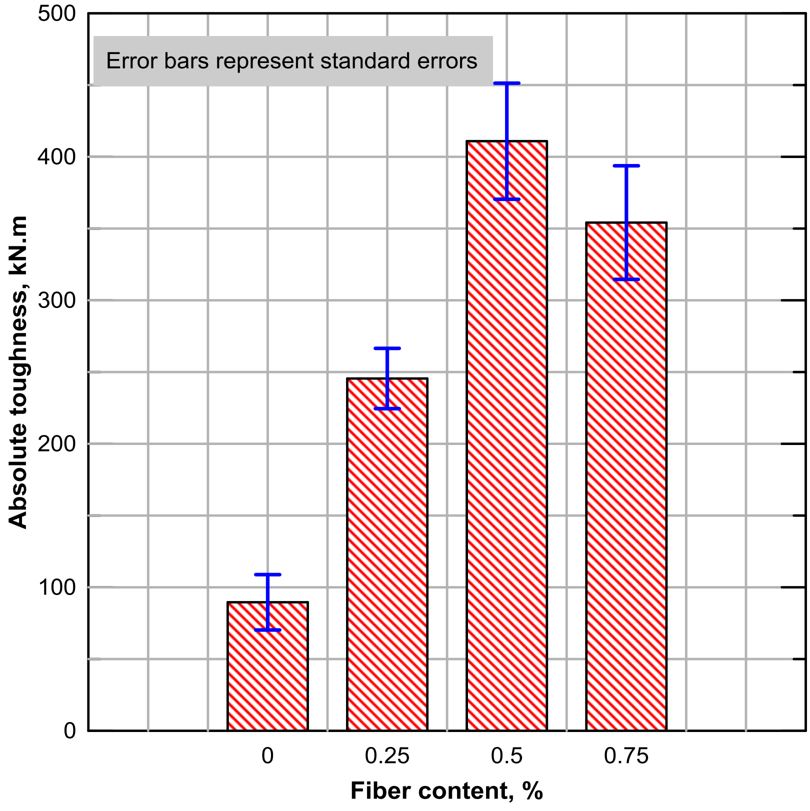

Figure 11: Deformability indices for various investigated mixtures.

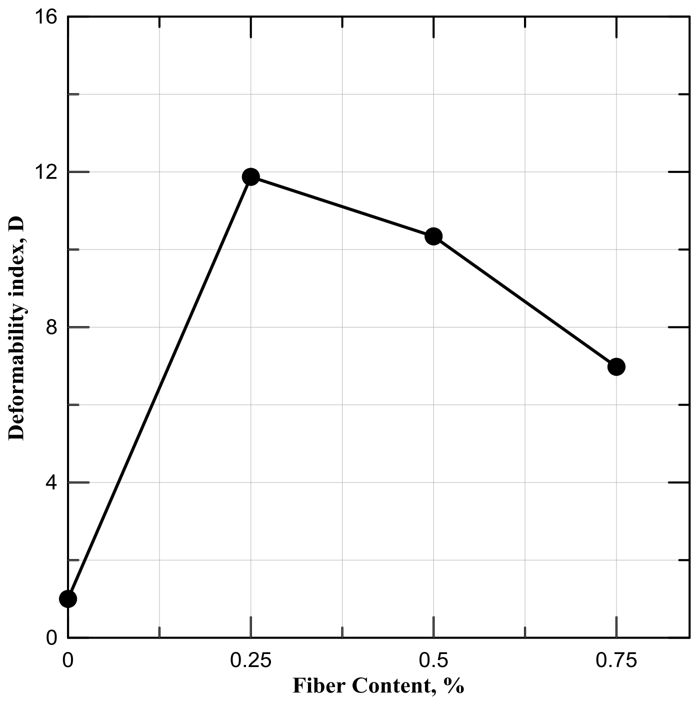

Figure 12: X-raying tensile-induced failed samples.

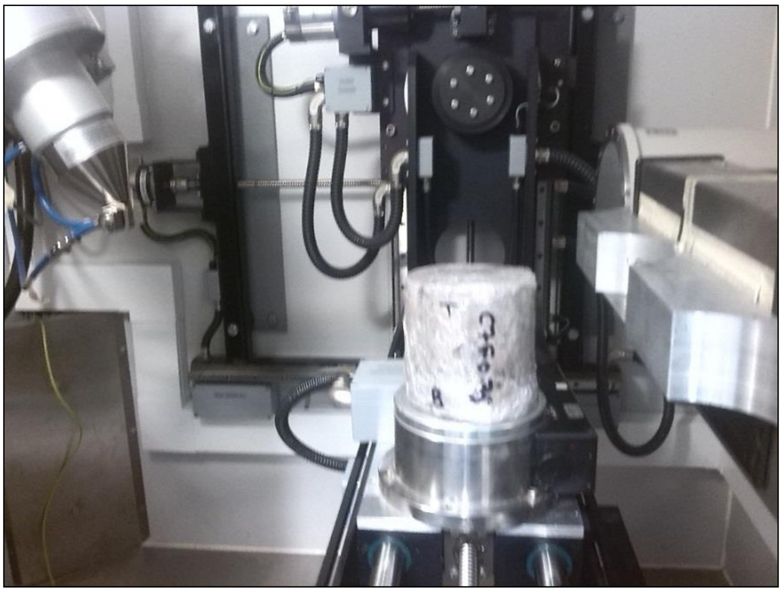

Figure 13: X-ray sample images of failed specimens: a. C7F0; b. C7F0.25; c. C7F0.5 and d. C7F0.75

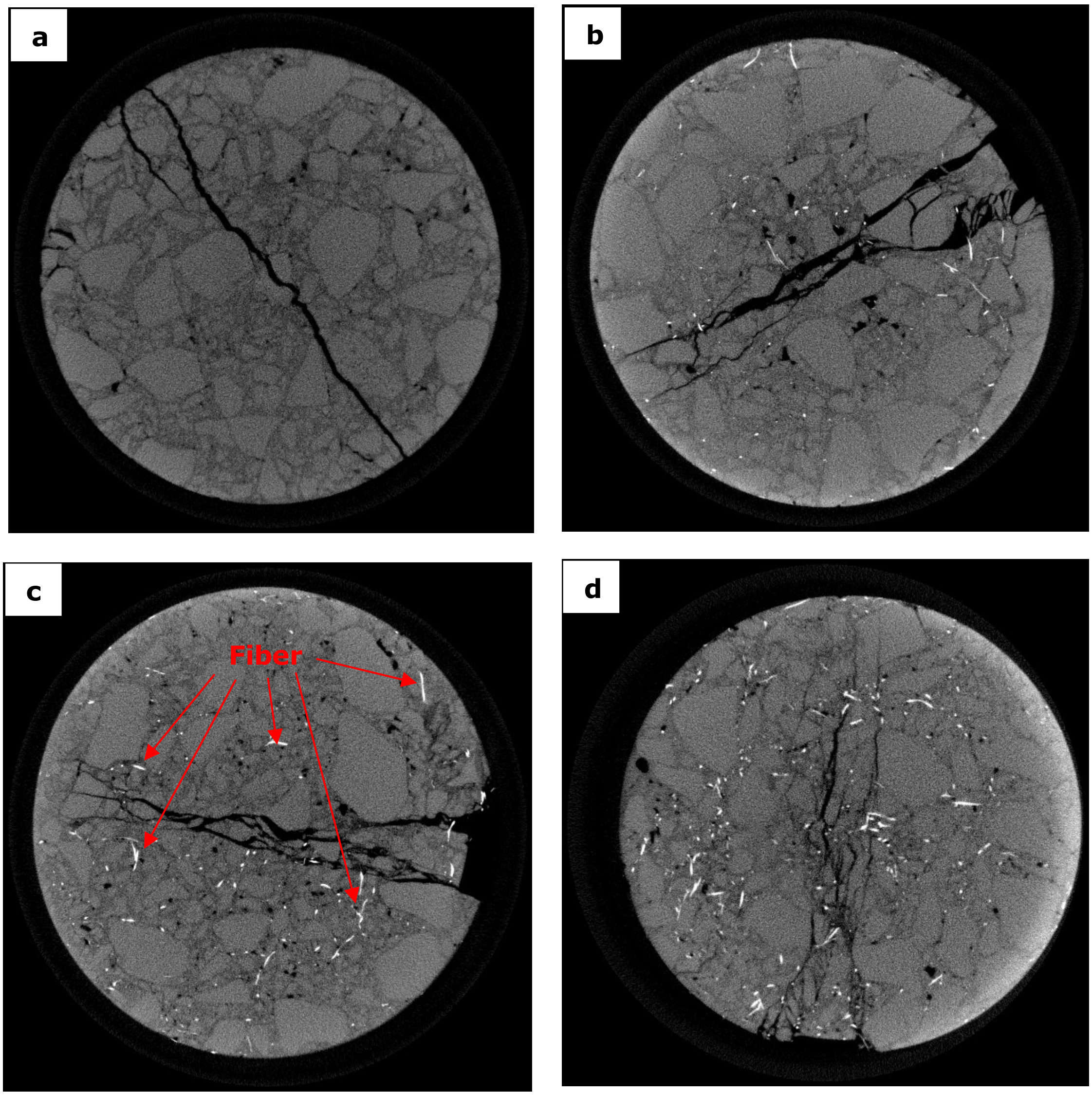

Figure 14: Failure modes for various investigated mixtures: a. C7F0.25; b.C7F0.5; c. C7R0.75.

Figure 15: Damage and mesostructure properties: a. Fiber distributions, b. cracking density distributions, c. fractal dimension distributions and d. Fracture energy distributions.

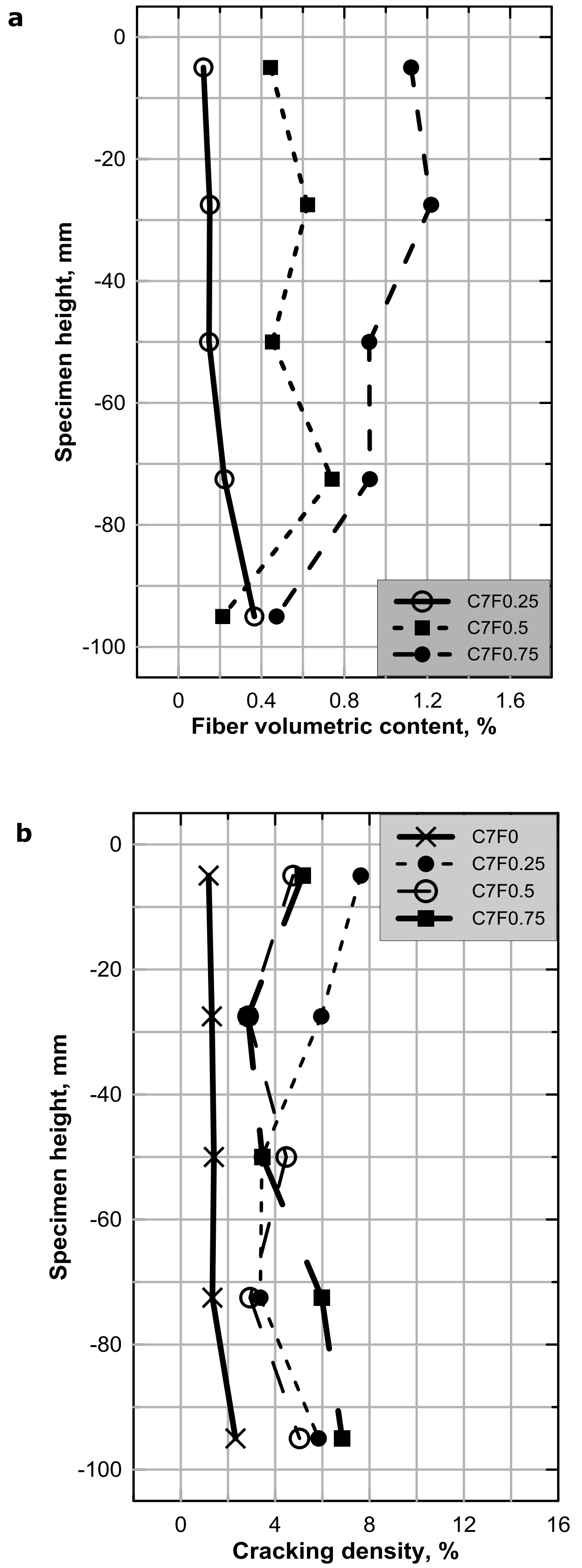

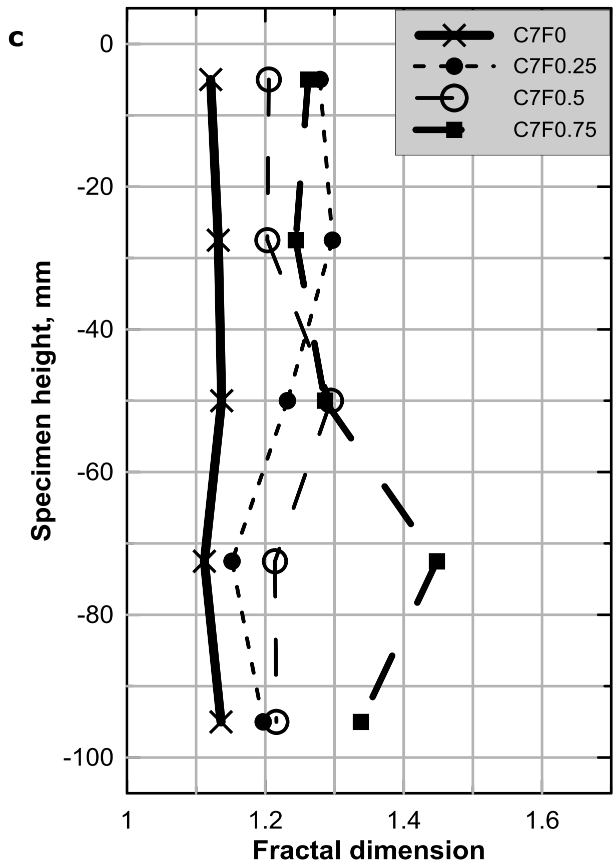
c
C7F0
C7F0.25
C7F0.5
C7F0.75
0
-20
-40
-60
-80
-100
Specimen height, mm
1
1.2
1.4
1.6
Fractal dimension

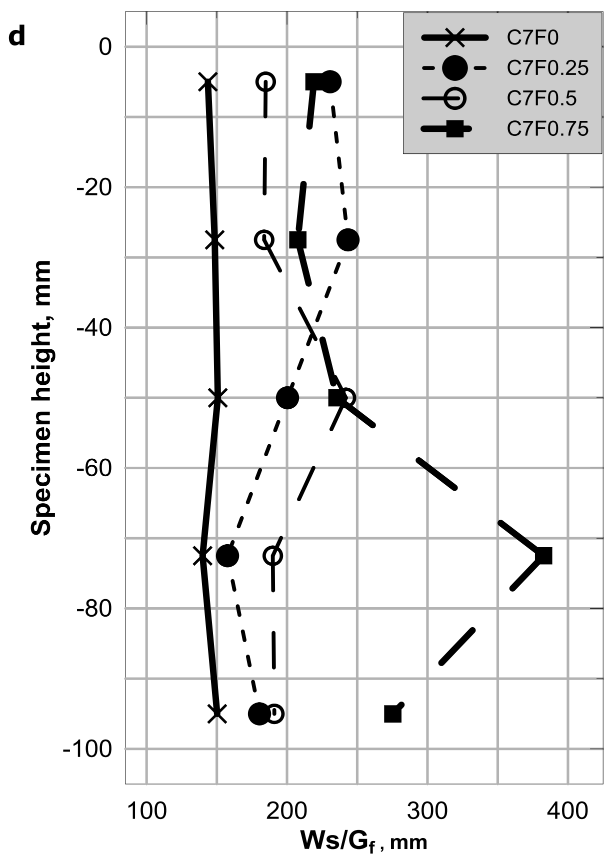
d
C7F0
C7F0.25
C7F0.5
C7F0.75
0
-20
-40
-60
-80
-100
Specimen height, mm
100
200
300
400
Ws/Gf , mm

Table 1: Average values of mesostructure properties for different fiber reinforcement levels.

Mixture designation	Fractal dimension	W_s / G_f, mm	Cracking density, %
C7F0	1.1276	146.62	1.50
C7F0.25	1.2314	202.52	5.20
C7F0.50	1.2266	198.27	4.01
C7F0.75	1.3156	264.10	4.86

Figure 16: Correlation of fractal dimension with ITS and elastic modulus.

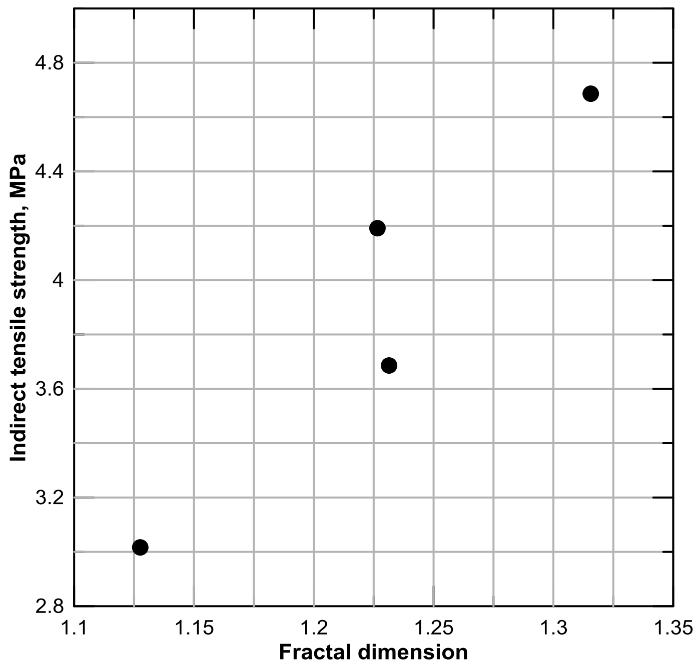

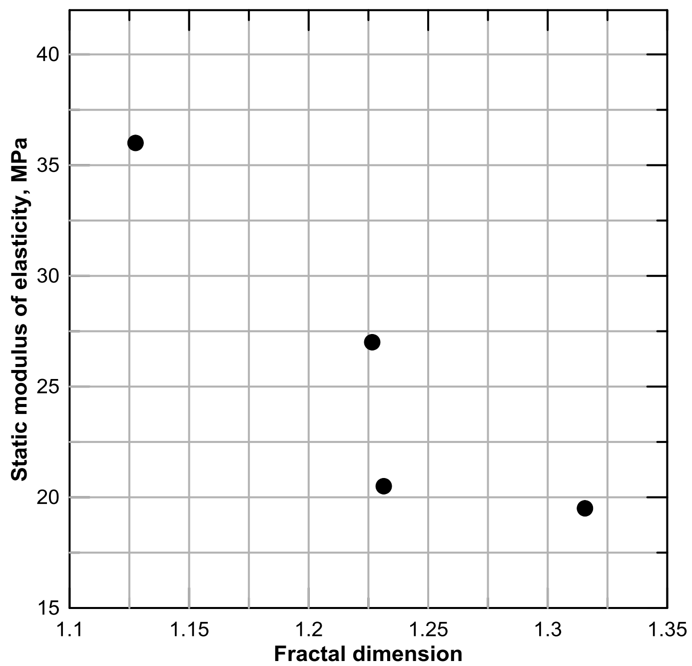

References

Adaska, W. S and Luhr, D. R. (2004). "Control of reflective cracking in cement stabilized pavements." in 5th International RILEM Conference on Cracking in Pavements – Mitigation, Risk Assessment and Prevention, ed. Petit, C., Al-Qadi, I. L. and Millien, A., Limoges, France, 309-316.

Adaska, W. S., Luhr D. R., Petit C., Al-Qadi I. L. and Millien A. (2004). Control of reflective cracking in cement stabilized pavements. Fifth International RILEM Conference on Reflective Cracking in Pavements, RILEM Publications SARL.

Aghaee, K., Yazdi M. A. and Tsavdaridis K. D. (2015). "Investigation into the mechanical properties of structural lightweight concrete reinforced with waste steel wires." Magazine of Concrete Research **67**(4): 197-205.

Aiello, M. A. and Leuzzi F. (2010). "Waste tyre rubberized concrete: properties at fresh and hardened state." Waste Manag **30**(8-9): 1696-1704.

Angelakopoulos, H., Papastergiou P. and Pilakoutas K. (2015). "Fibrous roller-compacted concrete with recycled materials – feasibility study." Magazine of Concrete Research **67**(15): 801-811.

Betterman, L., Ouyang C. and Shah S. (1995). "Fiber-matrix interaction in microfiber-reinforced mortar." Advanced Cement Based Materials **2**(2): 53-61.

Caggiano, A., Folino P., Lima C., Martinelli E. and Pepe M. (2017). "On the mechanical response of Hybrid Fiber Reinforced Concrete with Recycled and Industrial Steel Fibers." Construction and Building Materials **147**: 286-295.

Caggiano, A., Xargay H., Folino P. and Martinelli E. (2015). "Experimental and numerical characterization of the bond behavior of steel fibers recovered from waste tires embedded in cementitious matrices." Cement and Concrete Composites **62**: 146-155.

Carpinteri, A., Chiaia B. and Invernizzi S. (1999). "Three-dimensional fractal analysis of concrete fracture at the meso-level." Theoretical and Applied Fracture Mechanics **31**(3): 163-172.

Centonze, G., Leone M. and Aiello M. A. (2012). "Steel fibers from waste tires as reinforcement in concrete: A mechanical characterization." Construction and Building Materials **36**: 46-57.

Coni, M. and Pani S. (2007). Fatigue analysis of fiber-reinforced cement treated bases. 4th International SIIV Congress. Palermo (Italy).

Erdem, S. and Blankson M. A. (2013). "Fractal–fracture analysis and characterization of impact-fractured surfaces in different types of concrete using digital image analysis and 3D nanomap laser profilometery." Construction and Building Materials **40**: 70-76.

Farhan, A. H., Dawson A. R. and Thom N. H. (2016). "Characterization of rubberized cement bound aggregate mixtures using indirect tensile testing and fractal analysis." Construction and Building Materials **105**: 94-102.

Farhan, A. H., Dawson A. R. and Thom N. H. (2016). "Effect of cementation level on performance of rubberized cement-stabilized aggregate mixtures." Materials & Design **97**: 98-107.

Grilli, A., Bocci M. and Tarantino A. (2013). "Experimental investigation on fibre-reinforced cement-treated materials using reclaimed asphalt." Construction and Building Materials **38**: 491-496.

Guo, L.-P., Sun W., Zheng K.-R., Chen H.-J. and Liu B. (2007). "Study on the flexural fatigue performance and fractal mechanism of concrete with high proportions of ground granulated blast-furnace slag." Cement and Concrete Research **37**(2): 242-250.

Hassan, N. A. (2012). Microstructural characterization of rubber modified asphalt mixtures PhD thesis, The university of Nottingham.

Issa, M. and Hammad A. (1994). "Assessment and evaluation of fractal dimension of concrete fracture surface digitized images." Cement and Concrete Research **24**(2): 325-334.

Khattak, M. J. and Alrashidi M. (2006). "Durability and mechanistic characteristics of fiber reinforced soil–cement mixtures." International Journal of Pavement Engineering **7**(1): 53-62.

Kim, S. B., Yi N. H., Kim H. Y., Kim J.-H. J. and Song Y.-C. (2010). "Material and structural performance evaluation of recycled PET fiber reinforced concrete." Cement and Concrete Composites **32**(3): 232-240.

Leone, M., Centonze G., Colonna D., Micelli F. and Aiello M. A. (2018). "Fiber-reinforced concrete with low content of recycled steel fiber: Shear behaviour." Construction and Building Materials **161**: 141-155.

Lim, S. and Zollinger D. G. (2003). "Estimation of the compressive strength and modulus of elasticity of cement-treated aggregate base materials." Transportation Research Record: Journal of the Transportation Research Board **1837**(1): 30-38.

Martinelli, E., Caggiano A. and Xargay H. (2015). "An experimental study on the post-cracking behaviour of Hybrid Industrial/Recycled Steel Fibre-Reinforced Concrete." Construction and Building Materials **94**: 290-298.

Neocleous, K., Angelakopoulos H., Pilakoutas K. and Guadagnini M. (2011). "Fibre-reinforced roller-compacted concrete transport pavements." Proceedings of the ICE-Transport **164**(TR2): 97-109.

Park, S.-S. (2011). "Unconfined compressive strength and ductility of fiber-reinforced cemented sand." Construction and Building Materials **25**(2): 1134-1138.

PCA (2005). "soil cement technology for pavement different products for different applications." Portland Concrete Association(illinois).

Sengul, O. (2016). "Mechanical behavior of concretes containing waste steel fibers recovered from scrap tires." Construction and Building Materials **122**: 649-658.

Shahid, M. A. (1997). "Improved Cement Bound Base Design for Flexible Composite Pavement." PhD Thesis, University of Nottingham.

Sobhan, K. and Krizek R. J. (1999). "Fatigue behavior of fiber-reinforced recycled aggregate base course." Journal of materials in civil engineering **11**(2): 124-130.

Sobhan, K. and Mashnad M. (2000). "Fatigue durability of stabilized recycled aggregate base course containing fly ash and waste-plastic strip reinforcement." Final Rep. Submitted to the Recycled Materials Resource Centre, Univ. of New Hampshire.

Sobhan, K. and Mashnad M. (2002). "Fatigue damage in roller-compacted pavement foundation with recycled aggregate and waste plastic strips." Transportation Research Record: Journal of the Transportation Research Board(1798): 8-16.

Sobhan, K. and Mashnad M. (2003). "Fatigue behavior of a pavement foundation with recycled aggregate and waste HDPE strips." Journal of geotechnical and geoenvironmental engineering **129**(7): 630-638.

Solanki, P. and Zaman M. (2013). "Behavior of Stabilized Subgrade Soils under Indirect Tension and Flexure." Journal of Materials in Civil Engineering **26**(5): 833-844.

Thompson, I. (2001). "Use of Steel Fibers to Reinforce Cement Bound Roadbase." PhD Thesis, University of Nottingham.

Yan, A., Wu K.-R., Zhang D. and Yao W. (2003). "Influence of concrete composition on the characterization of fracture surface." Cement and Concrete Composites **25**(1): 153-157.

Yan, A., Wu K. and Zhang X. (2002). "A quantitative study on the surface crack pattern of concrete with high content of steel fiber." Cement and Concrete Research **32**(9): 1371-1375.

Yang, W.-r., He X.-j. and Dai L. (2017). "Damage behaviour of concrete beams reinforced with GFRP bars." Composite Structures **161**: 173-186.

Zhang, P. and Li Q. (2009). "Effect of polypropylene fibre on mechanical and shrinkage properties of cement-stabilised macadam." International Journal of Pavement Engineering **10**(6): 435-445.

Zhang, P., Li Q. and Wei H. (2010). "Investigation of flexural properties of cement-stabilized macadam reinforced with polypropylene fiber." Journal of Materials in Civil Engineering **22**(12): 1282-1287.